Introduction

In seismic-while-drilling (SWD) operations, the vibrations produced by the drill bit are recorded using the seismic sensors located on the surface or in the nearby wells, and are then used for the imaging of the subsurface. The source signal produced by the drill bit is of a stochastic nature; it is hard to model or extract from the data. A traditional SWD processing workflow involves the direct recording of drill bit vibrations. These vibrations are then used for cross-correlation and deconvolution of seismic data, similar to vibroseis processing (Poletto and Miranda, 2004).

The sensors that record the vibrations produced by the drill bit can be placed on the top drive or downhole, near the bit. There is a difference between these sensors. The top drive data is readily available in real time and is synchronized to a GPS clock. Near-bit data can be available in real time only when fast real-time telemetry, such as wired drillpipe technology, is utilized. In other cases, near-bit sensors can solely rely on the internal clock, which is susceptible to significant drift. The data can only be extracted from such sensors after the bottomhole assembly (BHA) is brought to the surface. Still, the near-bit accelerometer is closer to the bit and may provide a better approximation of the signal radiated into the subsurface.

Time-variant cross-correlation (TVCC) analysis was shown to be effective for correcting a small drift of the near-bit sensor clock in SWD (Naville et al., 2004). In the field dataset that we analyze, the downhole clock drift is very high, around 0.04%. Time-variant cross-correlation can be applied to such data. Still, the drift at the end of the drilling run can reach 30 minutes, so the cross-correlation analysis, in this case, requires large time windows, which may influence the accuracy of the identified drift. We propose to apply an additional global optimization-based preprocessing step for the removal of the linear component of the clock drift and follow this step by traditional TVCC in small 30-second windows to remove the remaining drift, including the nonlinear component. For the study, we use an SWD dataset recorded during the first field test of the DrillCAM technology, where the drill bit vibrations were recorded by top-drive and downhole sensors and a set of surface seismic receivers (Bakulin et al., 2019). We use the top drive sensor to compensate for the drift of the near-bit sensor and apply both sensors' recordings for the deconvolution of the SWD data and compare the resulting gathers.

Method

The first step of our time-alignment methodology is a global optimization step to remove the linear component of the clock drift. We search for two scalar parameters – drift d and shift s – to create a linear mapping between the time vector for the near-bit acceleration recording and the synchronized top-drive time:

$$t^{td} = (1 + d)t^{nb} + s;\ t^{nb} = (t^{td} - s)/(1 + d). \quad (1)$$

Here, t^{td} and t^{nb} are the time vectors for the top-drive and near-bit sensors, both having the same origin, which is the moment of battery installation in the near-bit sensor. Value $d = 0$ and $s = 0$ would mean that the near-bit clock is entirely accurate.

We can directly look for such d and s that minimize the L2 misfit of waveform difference in the recorded top-drive and near-bit accelerations. Here, we use only vertical components of accelerations, $a_z^{td}(t^{td})$ for the top-drive sensor and $a_z^{nb}(t^{nb})$ for the near-bit sensor:

$$\sum_{t^{td}}(a_z^{td}(t^{td}) - a_z^{nb}((t^{td} - s)/(1 + d))^2 \rightarrow min \quad . \quad (2)$$

This requires an interpolation/resampling step for the near-bit sensor for each misfit calculation, so conducting any kind of optimization is costly given the fact that we use a 500 Hz sampling rate and tens of hours of recording. In addition, using the waveform misfit can further be complicated by potential

differences in the phase characteristics of two sensors. Instead, we choose to compute a specific attribute from the initial accelerations on a decimated time grid and use this attribute for optimization. Any attribute can be considered; here we use the total energy of vibrations (sum of squares of samples) in time windows, E^{td} and E^{nb} for top-drive and near-bit sensors, respectively. We compute E^{td} and E^{nb} in the seismic frequency band, after filtering the accelerations by a suitable bandpass filter (Ormsby bandpass with 15-25-40-80 Hz for the examples below). So, we look for $\hat{d}$ and $\hat{s}$ that minimize the following misfit:

$$J(d,s) = \sum_{t^{td}} \left(E^{td}\left(t^{td}_{dec}\right) - E^{nb}\left((t^{td}_{dec} - s)/(1+d)\right)\right)^2; \qquad \hat{d},\hat{s} = argmin\, J(d,s) \ . \tag{3}$$

Here, $_{dec}$ subscripts stand for decimation to the chosen size of the time window (30 s in our case). To minimize the misfit, we use a constrained grid search. From our experience, this misfit has a single minimum for reasonable values of drift and shift, which will be demonstrated for a field example below.

After the linear correction of the time vector with the identified $\hat{d}$ and $\hat{s}$, we conduct the conventional TVCC analysis in time widows with 30 s length. We divide the top-drive and near-bit sensors' recordings into time windows and perform direct cross-correlation. The lag of the cross-correlation's maximum identifies the remaining drift that needs to be corrected. This method allows for the correction of nonlinear drift. These residual corrections are often on the order of a few seconds.

After these two steps, the top and near-bit datasets are correctly aligned. It remains to account for the wave propagation time in the drillstring by introducing specific static corrections into the recordings of the sensors (Poletto and Miranda, 2004).

Field data example

Figure 1a compares a segment of top-drive energy (blue line) to near-bit energy before (orange line) and after time alignment with obtained $\hat{d}$ and $\hat{s}$ (green line). A small 7-point median filter was applied to the energies to remove outliers. Low levels of energy correspond to the periods when there is a pause in the drilling process. The timing inconsistency between the top drive and uncorrected near-bit energies can be clearly identified and is eliminated by the correction. Figure 1b shows the misfit for the used range of values of d and s (±1% for d and ±6 minutes for s). There is only one minimum that can be clearly identified. Note that alternative global optimization techniques can be used, such as simplex optimization.

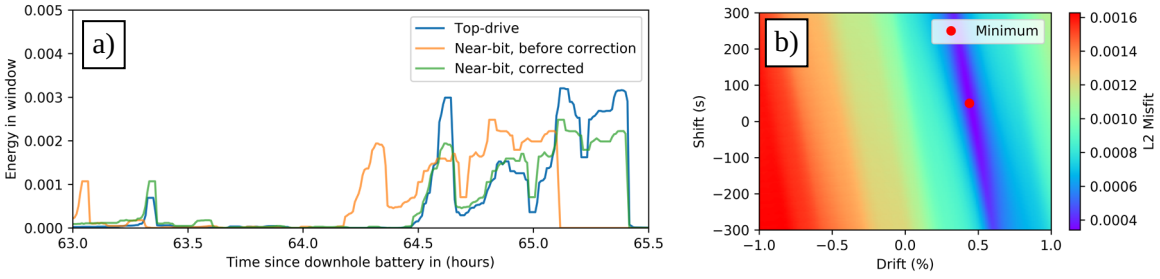

Figure 1 *(a) Top-drive (blue), near-bit uncorrected (orange) and near-bit corrected (green) energies in 30 s time windows. (b) A misfit function computed for a range of values of drift and shift; the minimum of the misfit function is highlighted with a red dot.*

It is important to note that the linear correction of drift is fully automatic and data driven. The linear correction brings the timing error down from tens of minutes to a few seconds. After this, the cross-correlation-based timing correction can be applied to remove the remaining errors. The cross-correlations between the top-drive and near-bit accelerations after the linear timing correction computed in 30 s-long time windows are shown in Figure 2a. The cross-correlation maxima (blue line in Figure

2a) show that the remaining component of drift is nonlinear. Using these picks, the residual drift can be corrected (Naville et al., 2004). Cross-correlations after the correction are displayed in Figure 2b. After the correction, the maxima of cross-correlations are aligned at the zero lag. Note the second high-amplitude event on the cross-correlations that has a staircase-like shape. This event corresponds to the cross-correlation between the direct wave propagating in the drillstring and the first-order multiple. The delay of this multiple is constant for a constant drillstring length. It changes when the drillpipes are added to the drillstring. The two-way analytical time in the drillstring was computed for this segment of drilling using the drillstring propagation velocity equal to 4960 m/s. It is displayed as a red line in Figure 2b and aligns well with the described event.

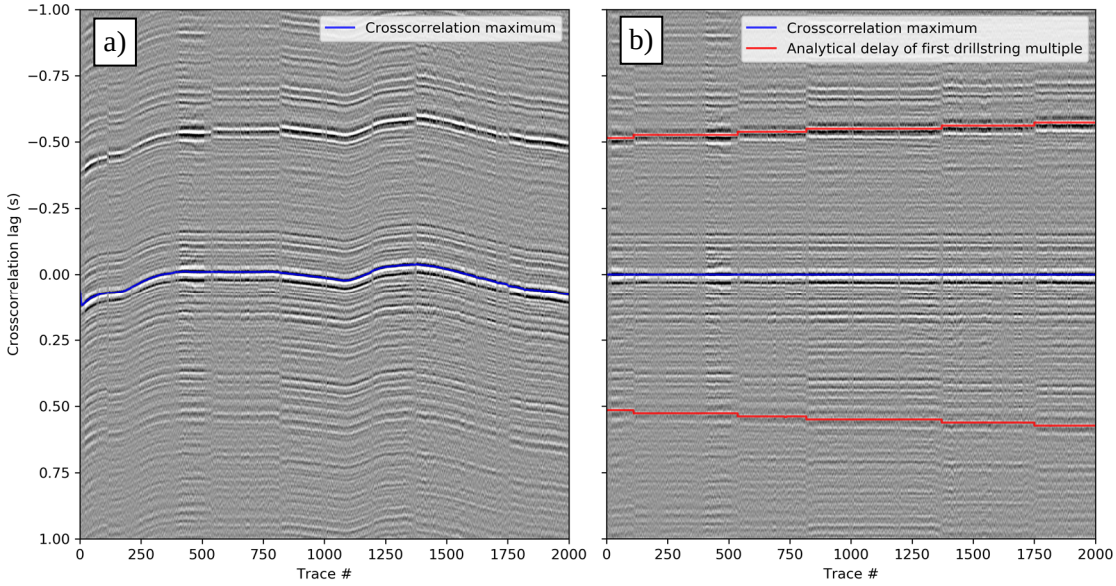

Figure 2 *Cross-correlation of the top drive and near-bit acceleration recordings before (a) and after (b) TVCC timing correction. Analytically computed delays of the first drillstring multiple are overlayed on the cross-correlation plot in (b). The depths of the displayed drilling segment are 1275-1390 m.*

After TVCC correction, the top-drive and near-bit sensors are correctly aligned. We can use the drillstring propagation time calculated from the multiple in Figure 2b to compute the remaining correction for the wave propagation in the drillstring and use the two sensors' recordings for the deconvolution of the surface seismic data. Figure 3 compares the seismic gathers deconvolved using the top-drive and near-bit sensor recordings. The bit depth is 1400 m. The same first arrivals can be identified on both gathers. Drillstring-related multiples manifest themselves as noncausal events (Rector and Marion, 1991). The differences in the recordings are caused by the different drillstring-related multiple patterns recorded by the top drive and downhole sensors (Poletto et al., 2001).

Conclusions

For the processing of seismic-while-drilling data, the clock accuracy similar to the surface seismic data sampling interval (on the order of millisecond) is required. The clock of the near-bit memory tool for vibration recording is not synchronized with GPS and is susceptible to significant drift, that complicates the processing of SWD data. A two-step alignment procedure consisting of a global optimization step and a time-variant cross-correlation analysis step successfully removes the drift as high as 0.04% for an SWD field data example. The seismic gathers are computed using the drill bit vibrations recorded by the top-drive and near-bit sensors. One can identify similar events (first arrivals and drillstring-related multiples) on these gathers.

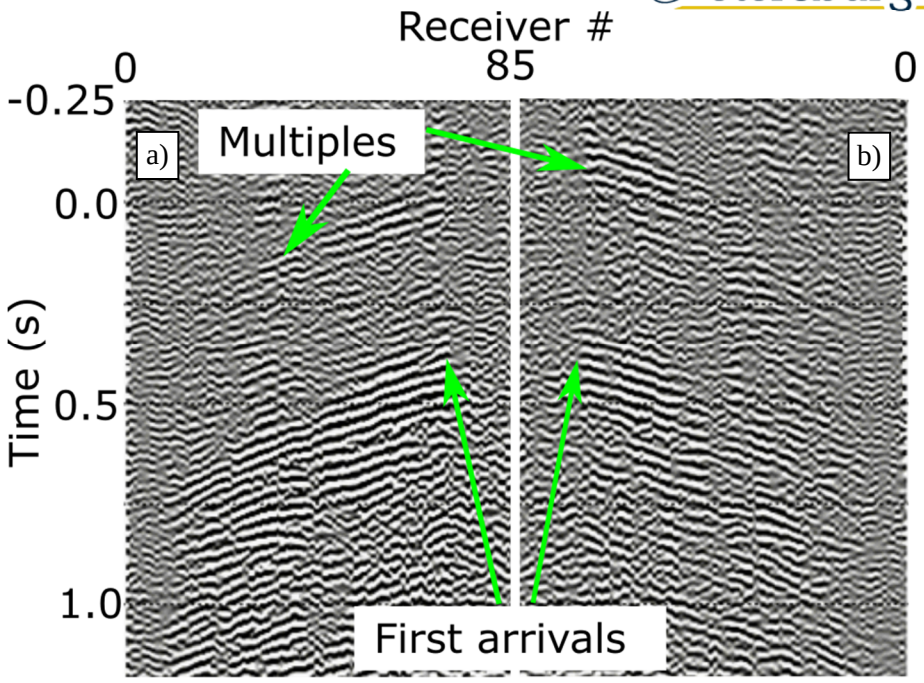

Figure 3 *Seismic gathers computed with the top drive (a) and near-bit (b) pilot sensor recordings. Gathers are mirrored with regards to each other for easier comparison of traveltimes.*

References

Bakulin, A., Hemyari, E., and Silvestrov, I. [2019]. Acquisition trial of DrillCAM: Real-time seismic with wireless geophones, instrumented top drive and near-bit accelerometer. *SEG Technical Program Expanded Abstracts 2019*, 157–161. https://doi.org/10.1190/segam2019-3214516.1

Naville, C., Serbutoviez, S., Throo, A., Vincké, O., and Cecconi, F. [2004]. Seismic While Drilling (SWD) Techniques with Downhole Measurements, Introduced by IFP and Its Partners in 1990-2000. *Oil & Gas Science and Technology*, *59*(4), 371–403. https://doi.org/10.2516/ogst:2004027

Poletto, F., Malusa, M., and Miranda, F. [2001]. Numerical modeling and interpretation of drillstring waves. *Geophysics*, *66*(5), 1569–1581. https://doi.org/10.1190/1.1487102

Poletto, F., and Miranda, F. [2004]. *Seismic While Drilling: Fundamentals of Drill-Bit Seismic for Exploration*. Elsevier.

Rector, J. W., and Marion, B. P. [1991]. The use of drill-bit energy as a downhole seismic source. *Geophysics*, *56*(5), 628–634. https://doi.org/10.1190/1.1443079